



Roof movement and instability fracture characteristics in shallow-buried thin coal seam conventional mining faces

Jihua Zhang · Qiao Rui · Yushun Yang ·
Jiarui Chen · Wei Shen · Yue Yuan ·
Chengwu Wang · Weili Liu

Received: 9 October 2023 / Accepted: 11 January 2024
© The Author(s) 2024

Abstract The variation in the width of the mining face significantly affects the stability of the face, leading to potential roof fracturing and collapse. Additionally, strong mining pressure can manifest, severely impeding the safe production of coal mines. This study uses the No. 16705 conventional working face of Jinda Coal Mine as its engineering background to investigate the characteristics of roof strata movement and instability under conditions of variable-width mining in shallow-buried thin coal seams. First, the dynamic load of the roof strata is estimated based on the key strata theory. Next, a mechanical model of the immediate roof strata movement in the working face is established based on the theory of elastic thin plates, which has been used to reveal the impact of different dimensions of the overhanging plate structure and residual overhanging structures in the corner on roof movement and its associated fracture mechanics. The findings indicated that the maximum bending deformation, deformation moment, and bending stress all have an exponential function relationship with the roof width. Similarly, these metrics have an

exponential function relationship with the overhanging span of the roof. In addition, these parameters all have a linear functional relationship with the size of the residual overhanging structures in the corner. Finally, the effect of roof instability on overlying pressure is analyzed, and both the initial fracture step length and cyclic movement fracture step length of the roof are estimated. These insights offer valuable scientific guidance and a theoretical foundation for analyzing the adaptability of load-bearing pillars pressure in thin coal seam mining faces, bearing significant relevance to safety production.

Highlights

1. A mechanical model was constructed by theory of the thin plate and the key layer that cloud analyze the initial and periodic roof breakages of conventional working face.
2. During the periodic roof breakage phase, the mechanical response of the roof's bending under stress was more obvious than the initial fracture stage.
3. The study can provide scientific guidance and technical support for the stability control of the working face roof and the selection of load-bearing pillars.

J. Zhang (✉) · Q. Rui · Y. Yang · J. Chen · W. Shen ·
Y. Yuan · C. Wang
Faculty of Architecture and Civil Engineering, Huaiyin
Institute of Technology, Huai'an 223001, China
e-mail: zhangjh84@hyit.edu.cn

W. Liu
School of Life Science and Food Technology, Huaiyin
Institute of Technology, Huai'an 223001, China

Keywords Thin coal seam · Conventional working face · Roof movement · Fracture characteristics · Theoretical analysis

1 Introduction

Underground coal mining is mainly influenced by complex geological conditions. Mining activities disrupt the original mechanical equilibrium of the rock mass, causing deformation of the surrounding rock, roof fractures, subsequent collapses, and strong mining pressure. These factors considerably impact the safety of coal mine operations. One primary cause of mining pressure manifestations in working faces is the instability of the overlying roof structure. Significant deformation and fracture mainly contribute to this instability. He et al. (2007) applied electromagnetic radiation technology to monitor and analyze the characteristics of roof fracture instability. Pang et al. (2022) used monitoring load data from hydraulic supports to predict roof disasters. Bu et al. (2022) established the mining induced bearing mechanical model to reveal the characteristics of impact from the strong mining pressure caused by the thick-hard roof breakage. Przyłucka et al. (2022) used Differential Interferometry Synthetic Aperture Radar and Persistent Scatterer Interferometry to monitor terrain subsidence disasters caused by roof fractures in Poland's Upper Silesian Coal Basin mining area. Wang and Lu (2022) used the theory of small deflection thin plate bending to establish and analyze four types of boundary conditions for the roof plate structure model, and adopted the adapted MATLAB and FLAC3D numerical simulation methods to analyze the roof plate fracture law and macroscopic mechanical response. To explain these manifestations, numerous scholars have proposed various theories and hypotheses (Song et al. 2017, 2019; Qian and Xu 2019; Qian 2017; Zuo et al. 2018), including the cantilever beam hypothesis, masonry beam hypothesis, and key strata theory.

The research on the movement characteristics of roofs in shallow-buried thin coal seam working faces has continued in recent years. Building on the key strata theory, Hou (2000, 2001) introduced the composite key strata theory. Xu et al. (2009) divided the key layer structure into single key layer and multiple key layers, and proposed that the mining damage in shallow-buried coal seams has

special characteristics primarily derived from single key layer structures. Zhao et al. (2020) examined the arching effect of pressure transmission in the roof strata under conditions of shallow-buried thin bedrock, focusing on fractures in overlying key strata. Zhou and Huang (2019) employed physical and numerical simulations to analyze the stability of the high-level inclined step rock beam structure in single-key strata and the inclined step rock beam and masonry beam structure in double-key strata on large mining height faces, demonstrating the mechanisms of rapid and cyclic pressures in single and double key strata working faces. Huang et al. (2017, 2019) utilized field measurements, physical similarity simulations, and theoretical analysis to explore the formation conditions of double-key strata in interlayered rock layers of shallow coal seams, as well as the stability of double key strata structures and methods for calculating support loads. Yuan et al. (2022) examined roof movement and stress in the surrounding rock of complex working faces with multiple key strata structures, utilizing the RFPA-Strata numerical simulation method to explore the fracture characteristics of different key strata pre- and post-fracture and the stress response of different key strata in broken conditions. Duan and Zheng (2022) investigated the roof movement and pressure patterns in the No. 42303 working face of a Shenhua mine, examining the movement and pressure patterns through physical and numerical simulations. Wei et al. (2022) conducted experiments and numerical simulations on overburden and surface damage in shallow coal seam mining under gullies. Zhang and Li (2021) assessed trends in support pressure changes and roadway stability during the mining process in shallow coal seams, recommending initial pressure step distances of 35–42 m and periodic pressure step distances of 13–16 m. Ren (2020) employed similarity simulation experiments to analyze the evolutionary process of full-thickness roof layer cutting events in shallow deep working faces, examining the interaction between working face supports and the roof and the spatiotemporal characteristics of full-thickness roof layer cutting. Hou et al. (2021) investigated the disturbance and fracture characteristics of overlying strata during over-gully mining of shallow coal seams, highlighting the vertical fractures appearing in the roof over the coal seam during mining. Wang et al. (2017)

combined experimental simulation, theoretical analysis, and field application methods to explore the fracture characteristics of old roofs in typical longwall mining of shallow coal seams, proposing the pillar method to adjust classical mechanical model parameters of old roof structures and refine mathematical models for support forces on the overburden. Zhao et al. (2017) investigated the fracture characteristics of overlying key strata and the manifestations of mining pressure during upslope mining of working faces in gully areas lacking key strata. Zhang et al. (2023) compared and analyzed the characteristics of balanced mining and roof movement patterns between the N00 mining approach and conventional mining methods, emphasizing the balanced mining attributes of the N00 method across four parameters: strata movement characteristics, strata damage coefficients, strata subsidence displacements, and strata crack progression. Ning et al. (2020) investigated the mechanical mechanism of overlying strata fracturing and the development of fractured zones during close-proximity coal seam group mining in the Gaojialiang coal mine, formulating a mechanical model for the secondary activation of broken overlying strata and ascertaining the associated mechanical activation conditions. Sun et al. (2019), grounded in the key strata theory and mechanical analysis of overburden, introduced a novel analytical solution named the analogous hyperbola subsidence model (AHSM) to portray the movement and damage of the internal burden. Ma et al. (2023) used indoor experiments and numerical analysis methods to study the key mechanisms controlling microcrack initiation and extension in layered and heterogenous rock masses which provided scientific basis for analysis of roof fracture in shallow buried coal seams. Tan et al. (2023) studied the stability of residual coal pillar mining in multi-seam mining, and established the linkage between the failure and instability of residual coal pillars and rock strata, and defined the boundary between two forms of failure, progressive versus dynamic which could guide the roof stability control of residual coal mining.

Based on the analysis above, scholars have produced research outcomes related to the roof movement characteristics of shallow-buried thin coal seam mining faces. However, studies on such faces' roof movement and instability fracture characteristics are

relatively limited. In addition, variations in face width affect the safety of the No. 16705 conventional working face at Jinda Coal Mine. This research examines the roof movement and instability fracture characteristics of shallow-buried thin coal seam conventional mining faces to address this issue, aiming to provide scientific support for safe production.

2 Analysis of mining load on roof strata

2.1 Engineering background

The mining operation at the No. 16705 conventional working face of Jinda Coal Mine targets the #16 coal seam, located at depths between 317.4 and 368.2 m. The coal seam averages approximately 1.0 m in thickness. The No. 16705 conventional working face lies on the eastern side of the seventh mining area, with unmined areas to its east, west, and within the seventh mining area. To its south is the goaf of the No. 16703 working face, while the F301 fault is to the north. This face operates as a single-face system, measuring an average of 1150 m in length and 93.8 m in width. The employed roof support system utilizes DW-type (external diameter 100 mm) single hydraulic column supports, complemented by on-site articulated roof beams and column supports. The single-end columns have shoes and caps that advance 1.2 m per cycle. The immediate roof is composed of gray limestone, and coal extraction occurs via the inclined longwall retreat mining method, where the total height from roof to floor is mined in one pass. The entire goaf roof is managed using the full-collapse method. The roof strata primarily consist of gray limestone, mudstone, and fine sandstone layers, with their physical and mechanical parameters presented in Table 1.

2.2 Analysis of mining load

Based on the theory of key strata controlled by rock layers, the dynamic loads supported by key strata are calculated using the following equation:

$$(q_n)_1 = \frac{E_1 h_1^3 (\gamma_1 h_1 + \gamma_2 h_2 + \dots + \gamma_n h_n)}{E_1 h_1^3 + E_2 h_2^3 + \dots + E_n h_n^3} \quad (1)$$

where h_i is the thickness of each rock layer ($i=1, 2, \dots, n$); γ_i is the volume density ($i=1, 2, \dots, n$); E_i is

Table 1 Physical and Mechanical Parameters of the Rock Strata

Serial number	Rock stratum	Rock stratum thickness/m	Bulk density/ kg/m ³	Elastic modulus/ GPa
1	Gray limestone	5.5	2600	1.6
2	Mudstone	0.7	2200	1.0
3	Gray limestone	0.55	2600	1.6
4	Mudstone	17	2200	1.0
5	Fine sandstone	9.7	2700	4.0
6	Gray limestone	2.1	2600	1.6
7	Mudstone	6.5	2200	1.0
8	Fine sandstone	5.4	2700	4.0
9	Gray limestone	4	2600	1.6
10	Mudstone	6	2200	1.0
11	Fine sandstone	10	2700	4.0

the elastic modulus ($i = 1, 2, \dots, n$). The first and n th rock layers deform synchronously in this equation, forming a composite beam.

Based on the definition and deformation characteristics of key strata, the overlying rock layers they control also deform in unison as the key strata deform. As a result, the loads they support are not required to be supported by the underlying rock layers. The first rock layer acts as the first key stratum, and its control range extends to the n th layer. Therefore, the $(n+1)$ th layer emerges as the second key stratum and must fulfill the subsequent condition:

$$q_{n+1} < q_n \quad (2)$$

$$l_n < l_{n+1} \quad (n = 1, 2, \dots, k) \quad (3)$$

where q_{n+1} and q_n are the loads borne by the first layer when calculating up to the $(n+1)$ th and n th layers, respectively; l_n represents the fracture distance of the n th layer, and k is the number of hard rock layers determined in the above equation.

Given the physical and mechanical parameters of the rock layers listed in Table 1, the self-load q_1 of the first layer, identified as the gray limestone layer, is calculated in the manner below:

$$q_1 = 143 \text{ kPa}, \quad (q_2)_1 = 158 \text{ kPa}, \\ (q_3)_1 = 172.3 \text{ kPa}, \quad (q_4)_1 = 28.1 \text{ kPa} < (q_3)_1$$

The first layer offers load-bearing assistance to the second and third layers but does not support the subsequent fourth layer.

The self-load q_4 of the fourth layer, recognized as a load-bearing layer, is computed as follows:

$$q_4 = 374 \text{ kPa}, \quad (q_5)_4 = 364.8 \text{ kPa}$$

The fourth layer consists of a 17 m thick mudstone. In contrast to the fifth layer, the 9.7 m thick fine sandstone, the fourth layer has reduced hardness and displays interlayer fractures. Thus, it does not offer load-bearing assistance to the layers above it.

The self-load q_5 of the fifth layer, designated as a load-bearing layer, is determined as follows:

$$q_5 = 261.9 \text{ kPa}, \quad (q_6)_5 = 315.2 \text{ kPa}, \\ (q_7)_5 = 425.7 \text{ kPa}, \quad (q_8)_5 = 483.5 \text{ kPa}, \\ (q_9)_5 = 554.2 \text{ kPa}, \quad (q_{10})_5 = 628.3 \text{ kPa}, \\ (q_{11})_5 = 600.8 \text{ kPa} < (q_{10})_5$$

This fifth layer comprises a 9.7 m thick fine sandstone with considerable hardness and thickness. It crucially supports several overlying rock layers, displaying distinct key stratum features in relation to its mechanical attributes.

Based on extensive prior research on coal seam mining, while the coal seam has a thickness of nearly 1 m, the roof strata display a hinging structural instability during mining-induced fracturing. The fifth layer, made up of fine sandstone with a thickness of 23.75 m from the coal seam's roof, surpasses the height of the mining-induced fracture zone associated with coal seam extraction. Its mining effect exerts minimal influence on the pillars of this face.

The most noticeable impact on the pillars within this face arises from the mining-induced instability and strata pressure of the 5.5 m thick gray limestone layer (first layer) and the 17 m thick mudstone layer (fourth layer). The fourth layer can impose initial and periodic pressures on the face pillars, potentially influencing the roof strata. In addition, with variable face widths, shifts in roof strata hanging dimensions affect the stability and safety of the face pillars. Thus, a dynamic analysis of the immediately hanging roof strata is crucial to uncover the mechanical principles behind roof movement and fracture influences in a varying-width face scenario. This examination will be a theoretical guide for ensuing research on mining impacts and the adaptability of roof support for the No. 16705 conventional working face in standard mining practices.

3 Analysis of roof movement and instability breakage theory

3.1 Mechanical model analysis before initial breakage of key strata

Most scholars considered the key layer structure of the overlying rock as a beam structure for research (Song et al. 2017, 2019; Qian and Xu 2019; Qian 2017; Zuo et al. 2018), and these achievements provide some ideas for the analysis of the paper model. Due to the fact that the mining area is a three-dimensional space, it is more realistic to consider the key layer structure of the overlying rock as a plate structure before the initial mining fracture (Jiang et al. 2016). When calculating elastic thin plates in elastic mechanics, it is required that the plane width is much larger than the thickness. For the process of coal mining, the length of the working face and the distance of the working face are much larger than the thickness of the key layer structure of the overlying rock. Therefore, the key layer structure in the overlying rock layer can be regarded as an isotropic elastic thin plate composed of uniform unit bodies. Therefore, the movement law of the key layer of overlying strata in coal mining can be studied by using the small deflection deformation method of elastic thin plates (Li 2017). When considering the mid-plane as the xy -plane with the z -axis pointing vertically downward, the elastic thin plate, upon bending, causes various points on the

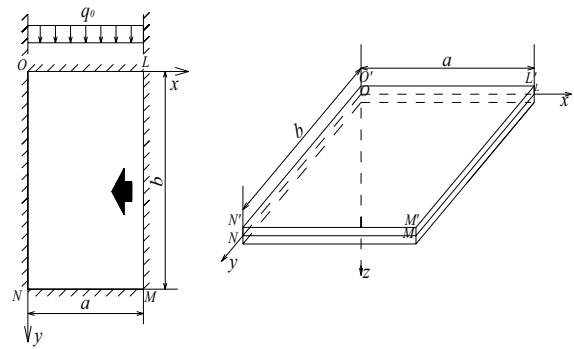


Fig. 1 Depicts the mechanical model before the initial fracture of the key layer

mid-plane to undergo a specific deflection $w(x, y)$ in the direction of the z -axis.

The key strata structure before the initial breakage can be visualized as the mechanical model shown in Fig. 1. It is assumed that the rectangular thin plate is rigidly supported on all four sides and subjected to a uniform load q (tensile stress is positive, compressive stress is negative). Here, a represents the span of the hanging roof strata, and b represents the width of the hanging roof strata. The boundary conditions are as follows:

Prior to the initial breakage, the key strata structure can be likened to the mechanical model presented in Fig. 1. This model assumes a rectangular thin plate, supported rigidly on all four sides and subjected to a uniform load q (where the tensile stress is positive while the compressive stress is negative). In this context, a denotes the span of the hanging roof strata, and b indicates the width of the hanging roof strata. The relevant boundary conditions are presented in the following section.

$$\left. \begin{aligned} w|_{x=0} = 0 & \quad \frac{\partial w}{\partial x}|_{x=0} = 0 \\ w|_{x=a} = 0 & \quad \frac{\partial w}{\partial x}|_{x=a} = 0 \\ w|_{y=0} = 0 & \quad \frac{\partial w}{\partial y}|_{y=0} = 0 \\ w|_{y=b} = 0 & \quad \frac{\partial w}{\partial y}|_{y=b} = 0 \end{aligned} \right\} \quad (4)$$

Based on these boundary conditions, Eq. (5) serves as the bending equation for the rectangular plate structure preceding the initial breakage of the key strata.

$$w = A_1 \sin^2 \frac{\pi x}{a} \sin^2 \frac{\pi y}{b} \tag{5}$$

Solving Eq. (5) yields:

$$\begin{cases} \frac{\partial^2 w}{\partial x^2} = A_1 \frac{2\pi^2}{a^2} \cos \frac{2\pi x}{a} \sin^2 \frac{\pi y}{b} \\ \frac{\partial^2 w}{\partial y^2} = A_1 \frac{2\pi^2}{b^2} \sin^2 \frac{\pi x}{a} \cos \frac{2\pi y}{b} \\ \frac{\partial^2 w}{\partial x \partial y} = A_1 \frac{\pi^2}{ab} \sin \frac{2\pi x}{a} \sin \frac{2\pi y}{b} \end{cases} \tag{6}$$

The general function of the plate structure is expressed as follows:

$$\Phi = \frac{D}{2} \iint \left(\frac{\partial^2 w}{\partial x^2} + \frac{\partial^2 w}{\partial y^2} \right)^2 - 2(1 - \mu) \left[\frac{\partial^2 w}{\partial x^2} \frac{\partial^2 w}{\partial y^2} - \left(\frac{\partial^2 w}{\partial x \partial y} \right)^2 \right] dx dy - \iint q w dx dy \tag{7}$$

where D is the flexural stiffness of the elastic thin plate, which can be obtained from the equation $D = Eh^3 / 12(1 - \nu^2)$; E is the elastic modulus of the key strata; h is the thickness of the key strata; ν is the Poisson's ratio; q is the load exerted on the key strata by the overlying strata.

Allowing $\frac{\partial \Phi}{\partial A} = 0$, and Eq. (6) can be rearranged as follows:

$$A = \frac{qa^4 b^4}{D\pi^4 [3b^4 + 3a^4 + 2a^2 b^2]} \tag{8}$$

The bending equation for the four-sided rigidly supported plate structure is as follows:

$$\begin{aligned} M_x &= -D \left(\frac{\partial^2 w}{\partial x^2} + \nu \frac{\partial^2 w}{\partial y^2} \right) \\ &= -2\pi^2 A_1 D \left[\frac{1}{a^2} \cos \frac{2\pi x}{a} \sin^2 \frac{\pi y}{b} + \frac{\nu}{b^2} \sin^2 \frac{\pi x}{a} \cos \frac{2\pi y}{b} \right] \end{aligned} \tag{9}$$

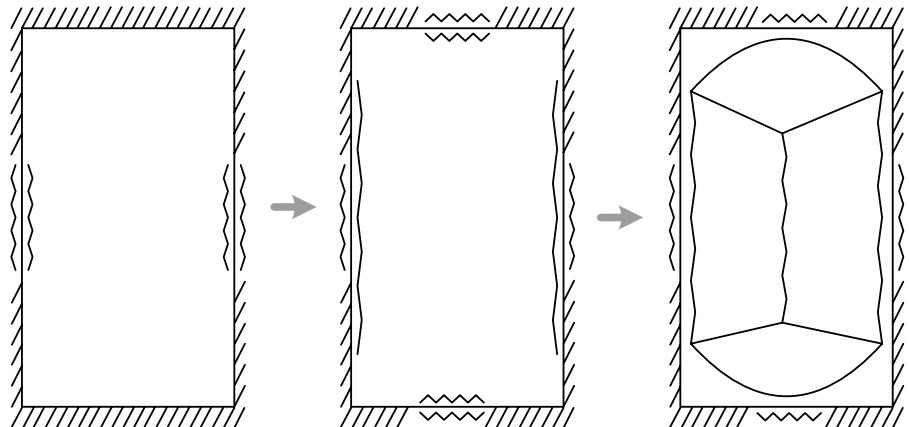
$$M_{x\text{Max}} = M_x \Big|_{x=0, y=\frac{b}{2}} = -\frac{2\pi^2 A_1 D}{a^2} = -\frac{2qa^2 b^4}{\pi^2 [3b^4 + 3a^4 + 2a^2 b^2]} \tag{10}$$

The maximum tensile stress strength theory is employed as the foundation for roof breakage in the mining region, namely $M_{x\text{max}} \geq -\frac{\sigma_h h^2}{6}$, where σ_h is the tensile strength of the roof strata in MPa.

3.2 Mechanical model analysis before the periodic breakage of key strata

Investigating the mining pressure and strata control theory reveals that fractures emerge when the hanging roof strata in a mining zone attain their maximum strength. For instance, in a mining area with a hanging roof supported on all sides, fractures first materialize at the center of the boundary on the lengthier sides, followed by the center of the boundary on the shorter sides. Ultimately, the surrounding fractures join to form an O-shaped crack pattern. Thereafter, fractures arise at the mid-bottom boundary of the plate, extending from the center of the plate towards its four corners, culminating in an X-shaped crack

Fig. 2 "O-X" fracture pattern of the roof (Qian and Xu 2019)



pattern. This progression results in the definitive O-X fracture pattern of the roof, as illustrated in Fig. 2.

Once the O–X fracture pattern manifests in the roof, triangular hanging plate structures linger at the four corners. These residual triangular hanging plates exert mechanical forces on the hanging roof, shaping an angular plate structure, as demonstrated in Fig. 3.

These remnants are equivalently modeled as rectangular hanging plate beam structures with equal areas to analyze the mechanical impact of triangular hanging plate remnants in the field, as depicted in Fig. 4. The analysis employs the principles of minimum potential energy and synchronous deformation.

Before the periodic breakage of the roof in the working area, the roof structure above the working

face is perceived as an elastic thin plate. When the mid-plane is used as the xy -plane and the z -axis is oriented vertically downward, the elastic thin plate experiences a specific deflection $w(x, y)$ in the z -axis direction when it bends. The mechanical influence of the triangular hanging plate remnants on the roof structure at the hanging end before periodic breakage is noted. As a result, the periodic roof structure simplifies to a three-sided supported and one-sided free periodic rectangular plate structure, synchronously deforming with the angular hanging plate beam structure. A subsequent mechanical analysis of the periodic roof structure of the key strata above the working face is conducted, as illustrated in Fig. 5.

Fig. 3 Illustrates the structural changes in the overlying rock key layers before and after mining

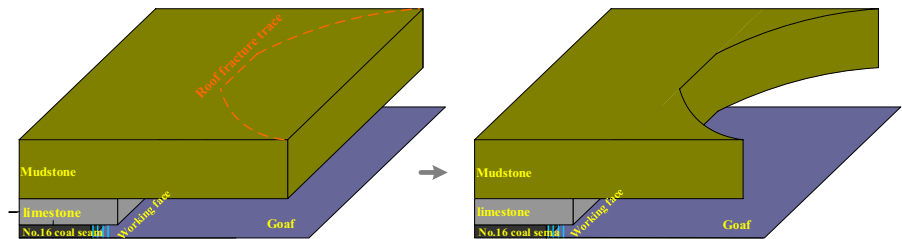
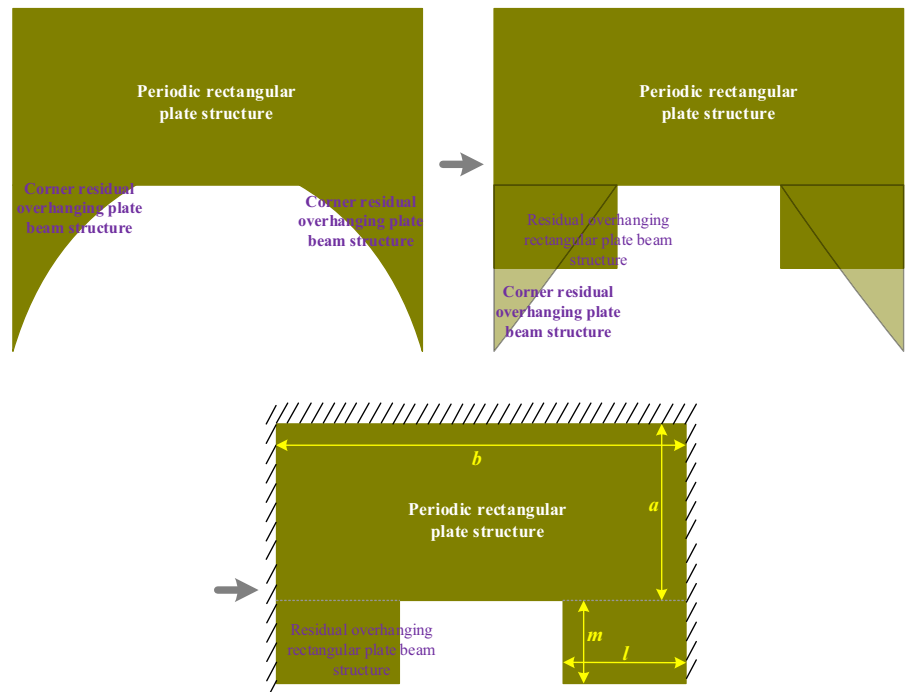


Fig. 4 The simplified cyclic roof structure



Boundary conditions for the periodic rectangular plate structure with three sides fixed and one side free:

$$\left. \begin{aligned} w|_{x=0} = 0 \quad \frac{\partial w}{\partial x}|_{x=0} = 0 \\ w|_{x=a} = 0 \quad \frac{\partial w}{\partial x}|_{x=a} = 0 \\ w|_{y=0} = 0 \quad \frac{\partial w}{\partial y}|_{y=0} = 0 \end{aligned} \right\} \quad (11)$$

The boundary conditions are established for a rectangular periodic plate structure with three sides fixed and one side free. Based on this structure and its boundary conditions, the following equation is chosen as the bending equation for the rectangular plate structure before periodic breakage in the key strata:

$$w = A \left(1 - \cos \frac{\pi x}{2a} \right) \left(1 - \cos \frac{2\pi y}{b} \right) \quad (12)$$

Based on the above equation, the following solution is obtained:

$$\left\{ \begin{aligned} \frac{\partial^2 w}{\partial x^2} &= \frac{\pi^2 A}{4a^2} \cos \frac{\pi x}{2a} \left(1 - \cos \frac{2\pi y}{b} \right) \\ \frac{\partial^2 w}{\partial y^2} &= \frac{4\pi^2 A}{b^2} \cos \frac{2\pi y}{b} \left(1 - \cos \frac{\pi x}{2a} \right) \\ \frac{\partial^2 w}{\partial x \partial y} &= \frac{\pi^2 A}{ab} \sin \frac{\pi x}{2a} \sin \frac{2\pi y}{b} \end{aligned} \right. \quad (13)$$

The function of the rectangular plate structure is represented as follows:

$$\Phi = \frac{D}{2} \iint \left\{ \left(\frac{\partial^2 w}{\partial x^2} + \frac{\partial^2 w}{\partial y^2} \right)^2 - 2(1 - \mu) \left[\frac{\partial^2 w}{\partial x^2} \frac{\partial^2 w}{\partial y^2} - \left(\frac{\partial^2 w}{\partial x \partial y} \right)^2 \right] \right\} dx dy - \iint q w dx dy - W_l \quad (14)$$

where W_l represents the equivalent work done for the rectangular hanging plate beam structure with equal areas.

When $W_l=0$, allowing $\frac{\partial \Phi}{\partial A} = 0$, the outcome is:

$$A = \frac{(\pi - 2)abq}{\pi \left[D\pi^4 \left[\frac{3b}{64a^3} + \frac{\pi - 4}{2\pi ab} + \frac{4(3\pi - 8)a}{\pi b^3} \right] + \frac{\pi^3(\pi + 4)(1 - \mu)D}{2ab} \right]} = \frac{64\pi(\pi - 2)a^4 b^4 q}{D[3\pi^6 b^4 + 32\pi^5(\pi - 4)a^2 b^2 + 256\pi^5(3\pi - 8)a^4 + 32\pi^5(\pi + 4)(1 - \mu)a^2 b^2]} \quad (15)$$

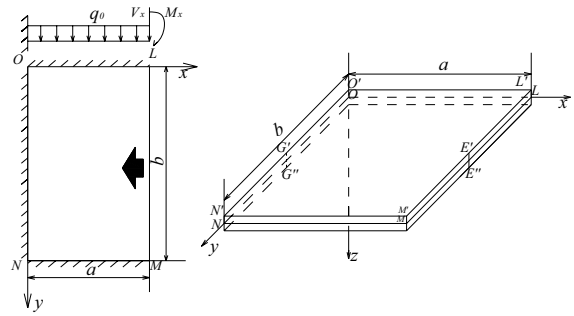


Fig. 5 Depicts the mechanical model before the key layer's cyclic failure

The corner's triangular hanging plate beam structure is equated with a rectangular hanging plate beam structure with matching areas. The hanging span in the mining face direction (x) and the lateral span in the transverse direction of the mining face (y) are labeled m and l , respectively. Establishing boundary conditions for this structure and based on the hanging rectangular plate beam structure with its conditions, the bending equation for the hanging rectangular plate beam structure is deduced:

$$w_l|_{y=0} = 0 \quad \frac{\partial w_l}{\partial y}|_{y=0} = 0 \quad (16)$$

Based on the hanging rectangular plate beam structure and its boundary conditions, the bending equation for the hanging rectangular plate beam structure is calculated as follows:

$$\frac{\partial^2 w_l}{\partial y^2} = \frac{\pi^2 B}{4l^2} \cos \frac{\pi y}{2l} \quad (17)$$

The function of the hanging rectangular plate beam structure is represented as:

$$\Phi = \frac{EI}{2} \int \left(\frac{\partial^2 w_l}{\partial y^2} \right)^2 dy - \int q w_l dy \tag{18}$$

where I represents the moment of inertia, namely $I = h^3/12$.

Under the action of a uniform load q and letting $\frac{\partial \Phi}{\partial A} = 0$, the following equation can be obtained:

$$B_q = \frac{32q l^4 (\pi - 2)}{EI \pi^5} \tag{19}$$

When the hanging rectangular plate beam structure and the rectangular periodic plate structure deform together, we consider $w_l(l) = w_l(a, l)$.

$$w_l = B_l \left(1 - \cos \frac{\pi y}{2l} \right) = w(a, l) = A \left(1 - \cos \frac{2\pi l}{b} \right) \tag{20}$$

$$A = \frac{\left[64a^4 b^4 (\pi - 2) - 128a^3 b^3 \pi l m \left(1 - \cos \frac{2\pi l}{b} \right) \left(\frac{\pi - 2}{\pi} \right) \right] q_0}{\pi^4 D \left[3\pi b^4 + 32a^2 b^2 (\pi - 4) + 256(3\pi - 8)a^4 \right] - \frac{8a^3 b^3 m EI \pi^5}{\beta^3} \left(1 - \cos \frac{2\pi l}{b} \right)^2} \tag{24}$$

Solved as:

$$B_l = A \left(1 - \cos \frac{2\pi l}{b} \right) \tag{21}$$

In other words, when the hanging rectangular plate beam structure and the rectangular periodic plate structure deform together, the equivalent load of the hanging rectangular plate beam structure is

$$M_{xMax} = M_x \Big|_{x=0, y=\frac{b}{2}} = -\frac{\pi^2 AD}{2a^2} \frac{\left[32a^2 b^4 (\pi - 2) - 64ab^3 \pi l m \left(1 - \cos \frac{2\pi l}{b} \right) \left(\frac{\pi - 2}{\pi} \right) \right] q}{\pi^2 \left[3\pi b^4 + 32a^2 b^2 (\pi - 4) + 256(3\pi - 8)a^4 \right] - \frac{8a^3 b^3 m EI \pi^3}{D \beta^3} \left(1 - \cos \frac{2\pi l}{b} \right)^2} \tag{26}$$

$$\begin{cases} B_l = \frac{32q_l l^4 (\pi - 2)}{EI \pi^5} = A \left(1 - \cos \frac{2\pi l}{b} \right) \\ q_l = \frac{AEI \pi^5}{32l^4 (\pi - 2)} \left(1 - \cos \frac{2\pi l}{b} \right) \end{cases} \tag{22}$$

At this point, the work done by the hanging rectangular plate beam structure on the rectangular periodic plate structure is determined by:

$$\begin{aligned} W_l &= \int q_l w_l dy - \int q_0 w_l dy \\ &= \left[\frac{AEI \pi^5}{32l^4 (\pi - 2)} \left(1 - \cos \frac{2\pi l}{b} \right) - q_0 \right] B_l \left(1 - \cos \frac{\pi y}{2l} \right) \end{aligned} \tag{23}$$

The following simplified form can be derived by substituting this above equation into the functional for the rectangular plate structure and letting $\frac{\partial \Phi}{\partial A} = 0$.

The bending equation for a rectangular plate structure with three sides fixed and one side free is:

$$\begin{aligned} M_x &= -D \left(\frac{\partial^2 w}{\partial x^2} + \mu \frac{\partial^2 w}{\partial y^2} \right) \\ &= -D \left[\frac{\pi^2 A}{4a^2} \cos \frac{\pi x}{2a} \left(1 - \cos \frac{2\pi y}{b} \right) + \nu \frac{4\pi^2 A}{b^2} \cos \frac{2\pi y}{b} \left(1 - \cos \frac{\pi x}{2a} \right) \right] \end{aligned} \tag{25}$$

Using the maximum tensile stress strength theory as the basis for the roof failure, namely $M_{x\max} \geq -\frac{\sigma_h h^2}{6}$. In the criterion, σ_h is the tensile strength of the roof rock, MPa.

4 Influence of different overhang structure sizes on roof movement and its fracture mechanics

Based on the preceding analysis, the study examines a 17 m thick mudstone roof, focusing on the influence of various overhang structure sizes on roof movement and fracture mechanics.

The initial assumptions are: the mudstone roof thickness is 17 m, the elastic modulus is 1.0 GPa, and the Poisson’s ratio is 0.2. Before the initial roof break, the overhang width was set to 30 m with 24 m periodic breaks. The roof experienced a load of 0.365 MPa. The periodic plate structure dimensions for the triangular overhang (both in the mining face direction (x) and transverse direction (y) are 10 m each. The study employed the plate bending deformation equations (Eqs. 5 and 11) and plate deformation moment equations (Eqs. 8 and 29) to assess the impact of different mining face widths on the initial and periodic roof movements and fracture patterns and the effect of varying overhang spans.

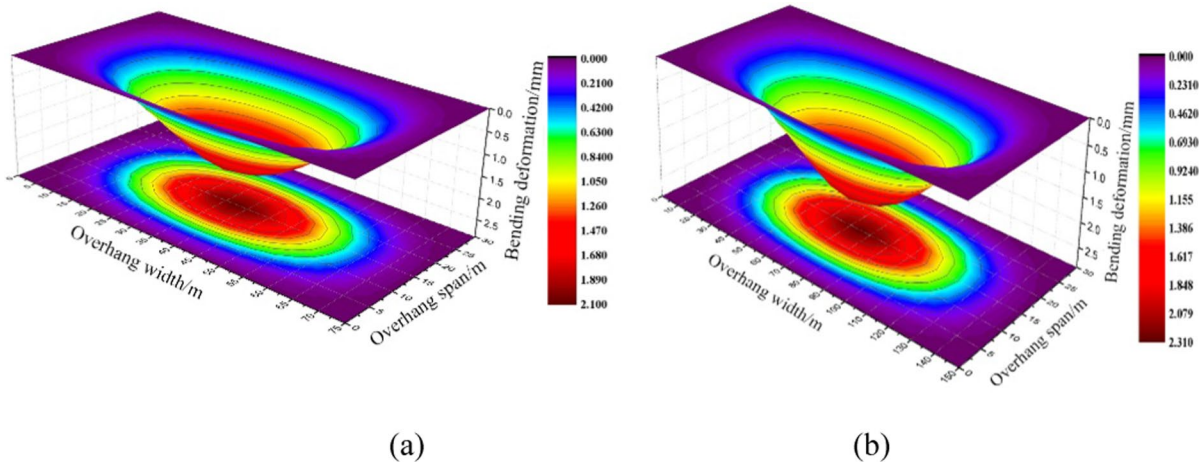


Fig. 6 Bending deformation characteristics of the roof under different overhang widths. **a** 75 m; **b** 150 m

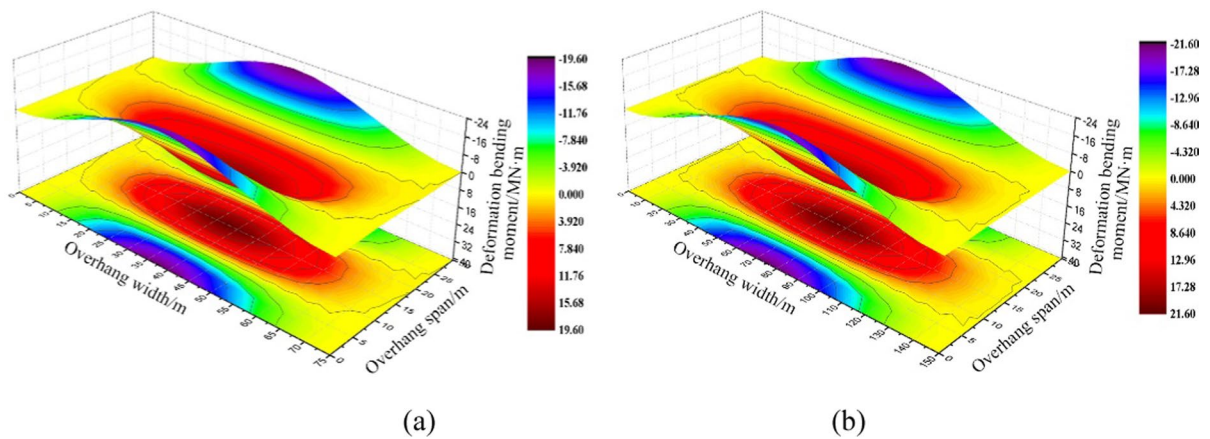


Fig. 7 Deformation bending moment characteristics of the roof under different overhang widths. **a** 75 m; **b** 150 m

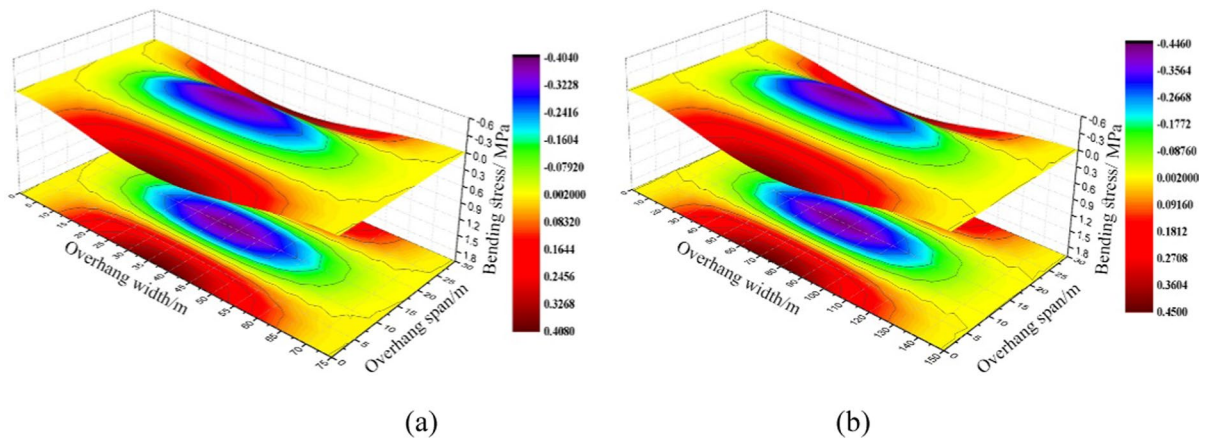


Fig. 8 Bending stress characteristics of the roof under different overhang widths. **a** 75 m; **b** 150 m

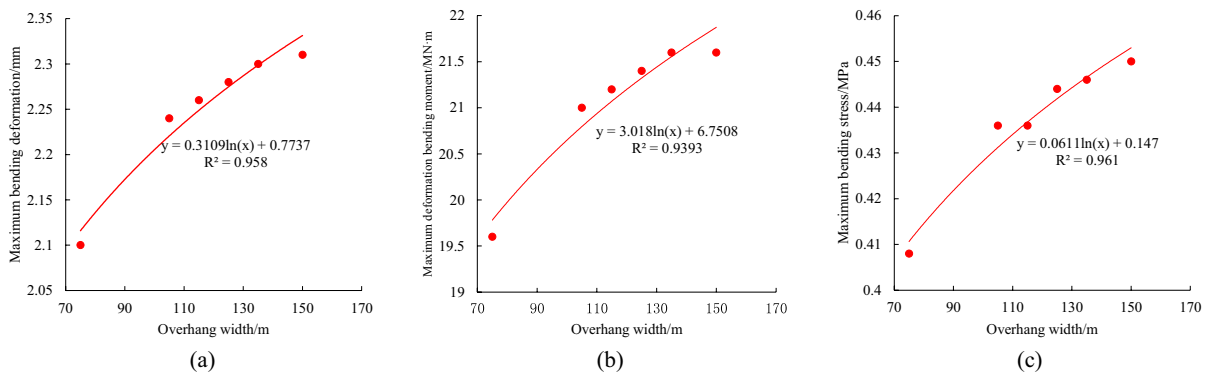


Fig. 9 Curves of maximum bending deformation, deformation bending moment, and bending stress as a function of overhang width. **a** bending deformation; **b** deformation bending moment; **c** bending stress

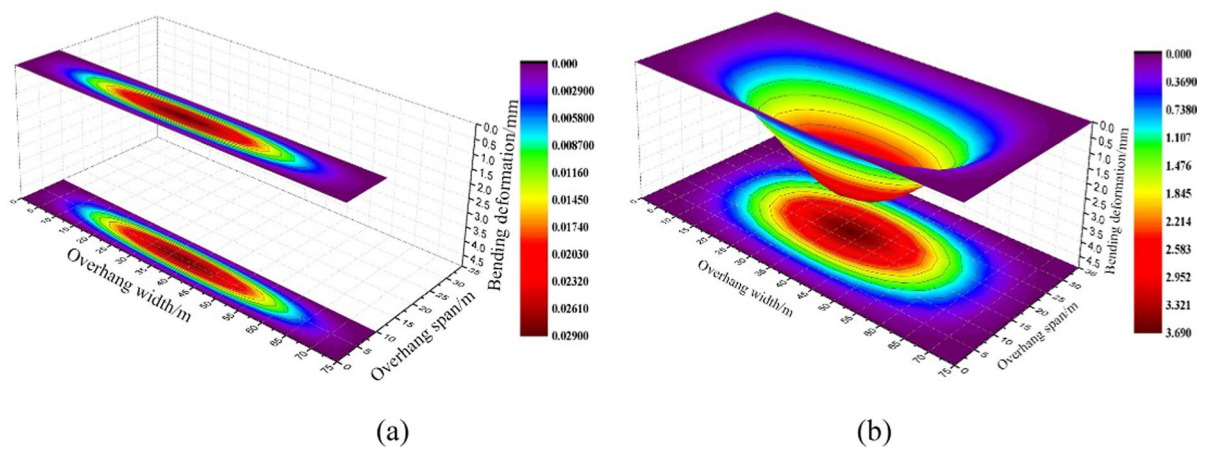


Fig. 10 Bending deformation characteristics of the roof under different overhang spans. **a** 10 m; **b** 35 m

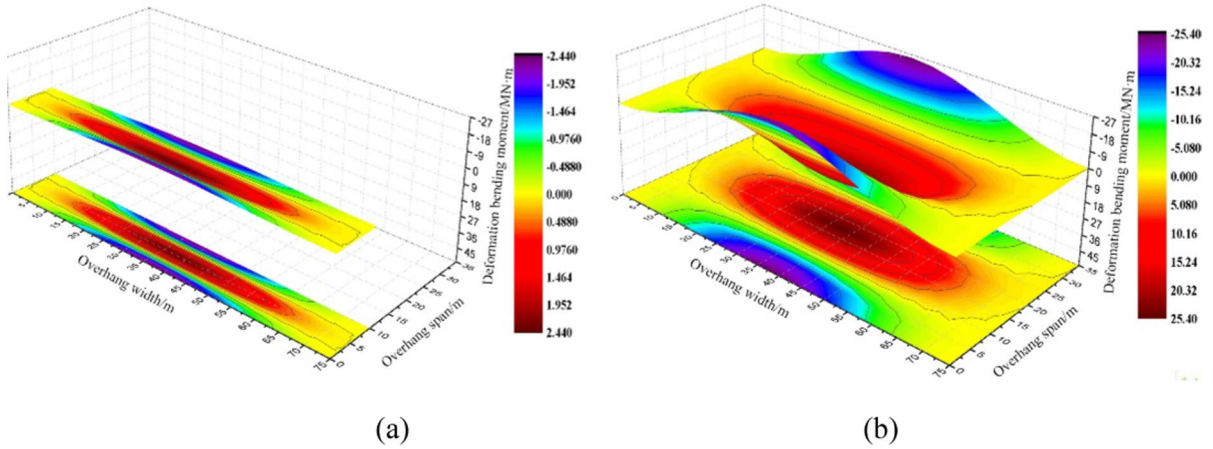


Fig. 11 Deformation bending moment characteristics of the roof under different overhang spans. a 10 m; b 35 m

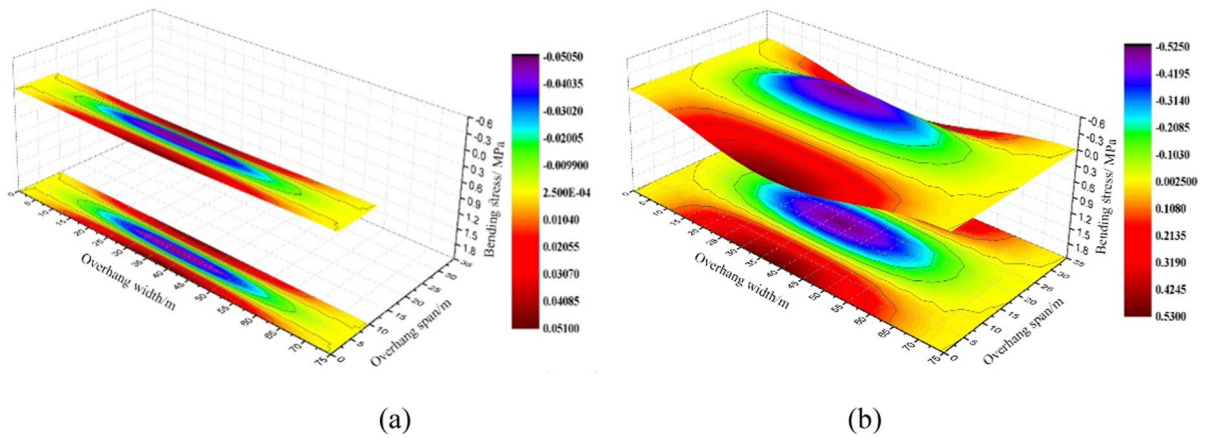


Fig. 12 Bending stress characteristics of the roof under different overhang spans. a 10 m; b 35 m

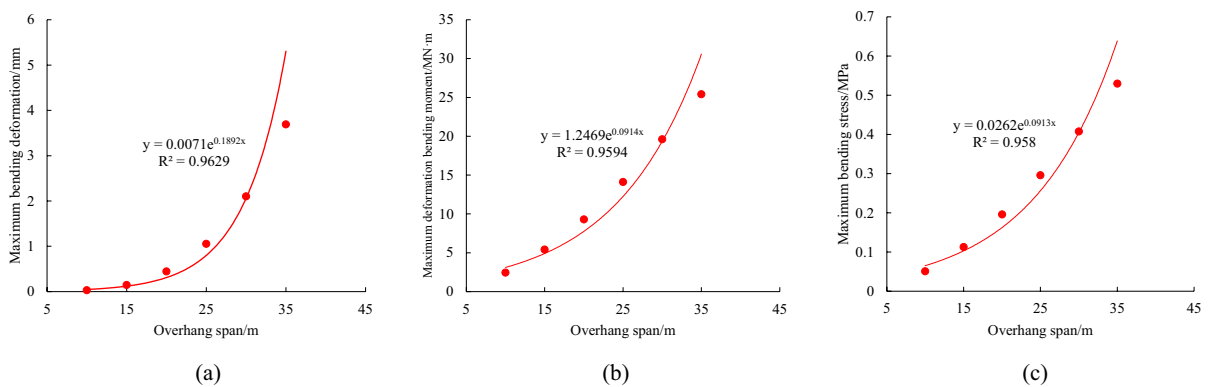


Fig. 13 Curves depicting the maximum bending deformation, deformation moment, and bending stress as a function of overhang span. **a** Bending deformation; **b** deformation bending moment; **c** bending stress

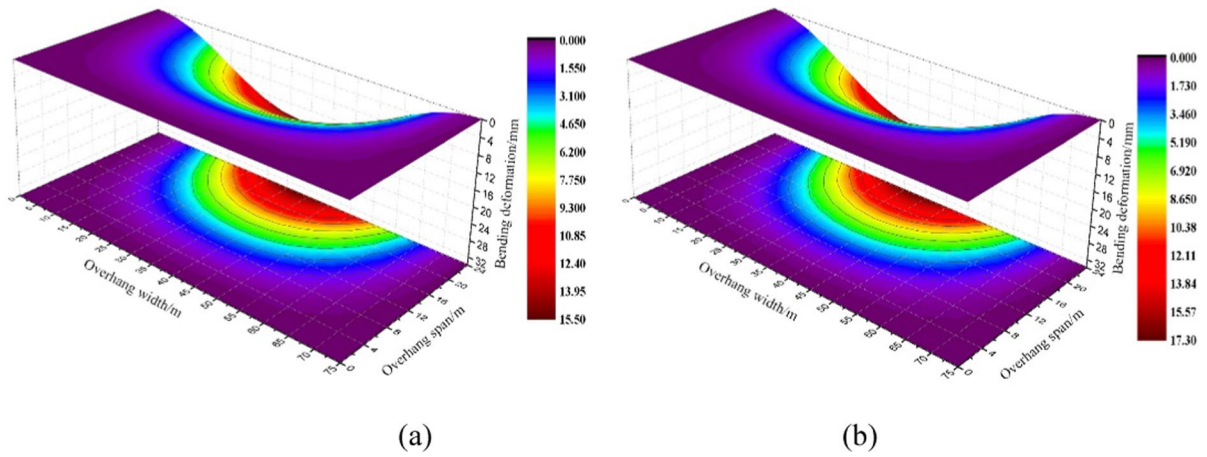


Fig. 14 Bending deformation characteristics of the roof along the horizontal overhang span. a $l=2$ m; b $l=10$ m

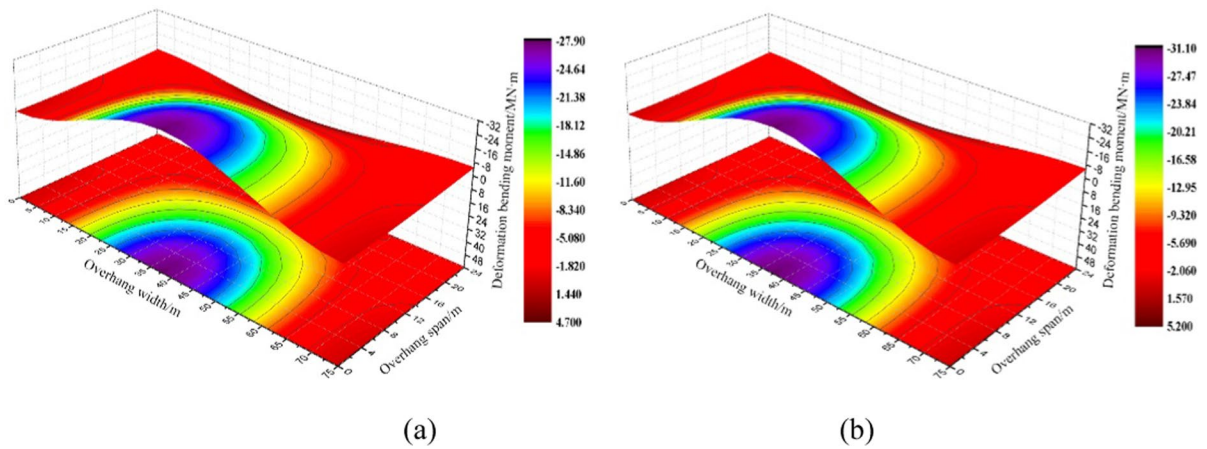


Fig. 15 Deformation bending moment characteristics of the roof along the horizontal overhang span. a $l=2$ m; b $l=10$ m

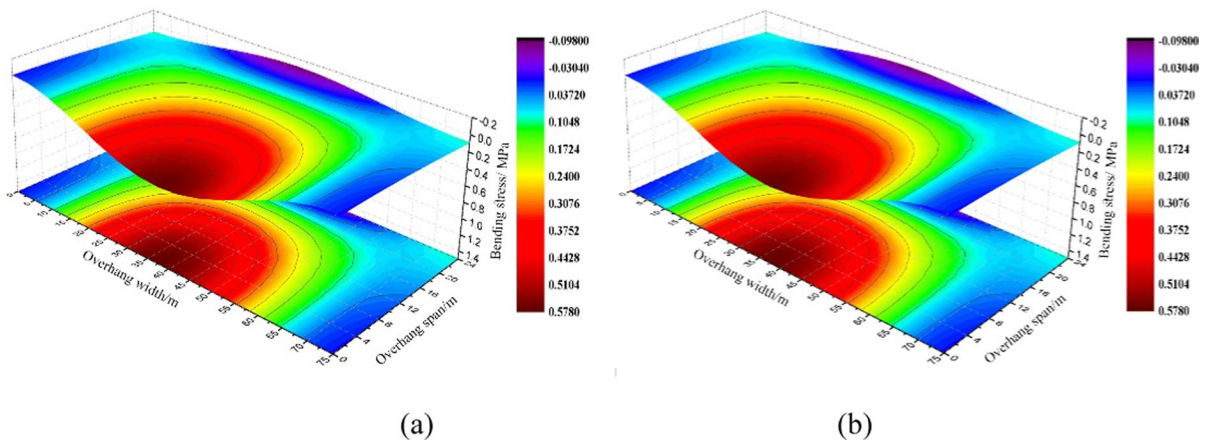


Fig. 16 Bending stress characteristics of the roof along the horizontal overhang span. a $l=2$ m; b $l=10$ m

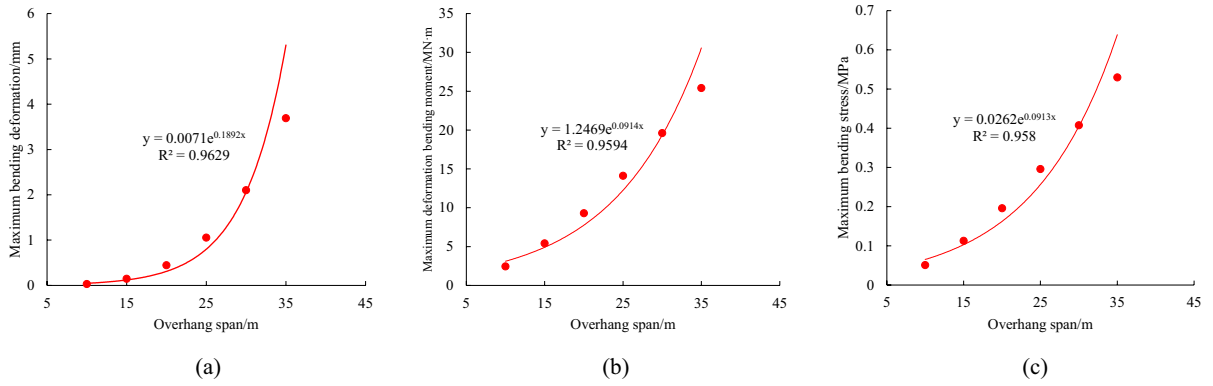


Fig. 17 Curves of maximum bending deformation, deformation bending moment, and bending stress as a function of the horizontal overhang span. **a** Bending deformation; **b** deformation bending moment; **c** bending stress

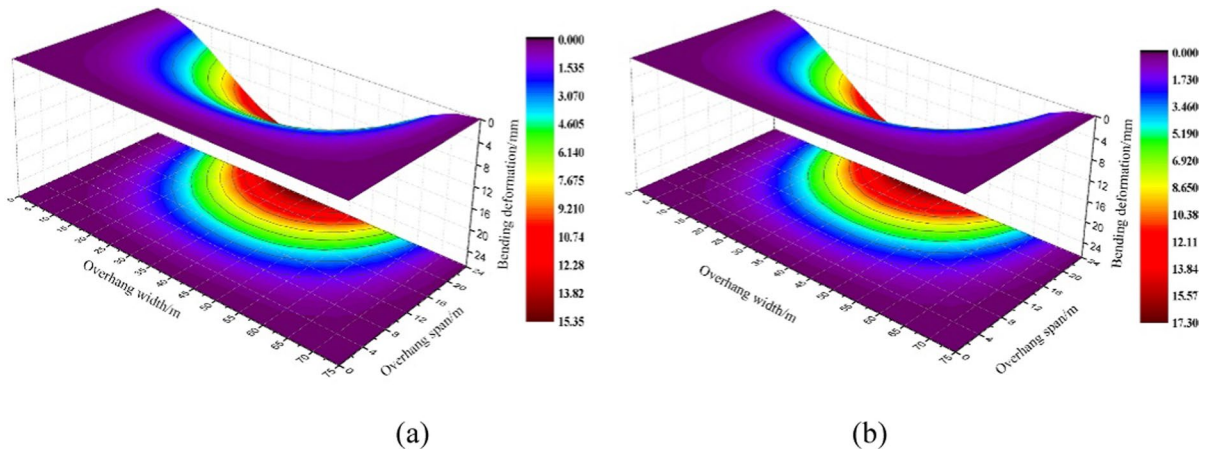


Fig. 18 Bending deformation characteristics of the roof along the trend overhang span. **a** $m = 2$ m; **b** $m = 10$ m

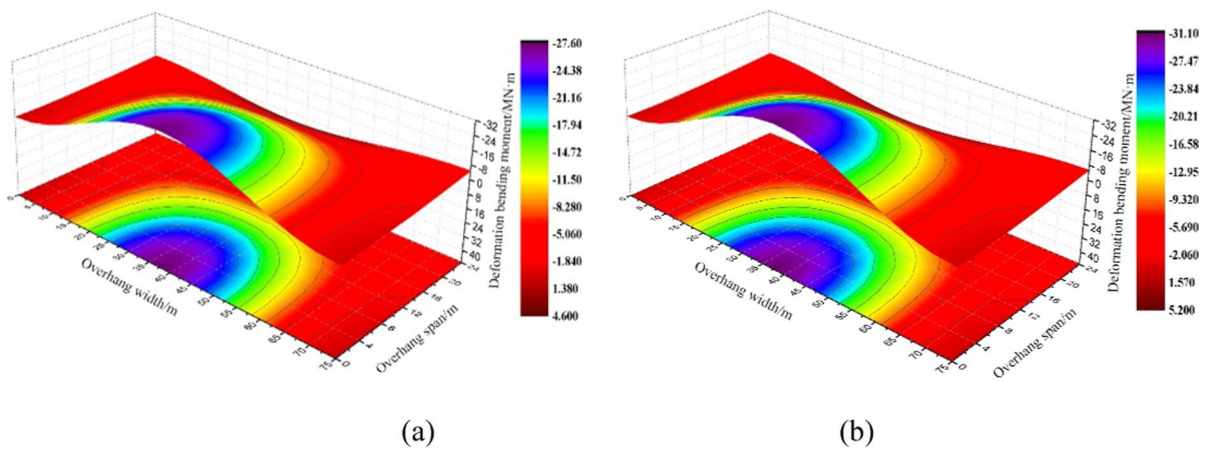


Fig. 19 Deformation bending moment characteristics of the roof along the trend overhang span. **a** $m = 2$ m; **b** $m = 10$ m

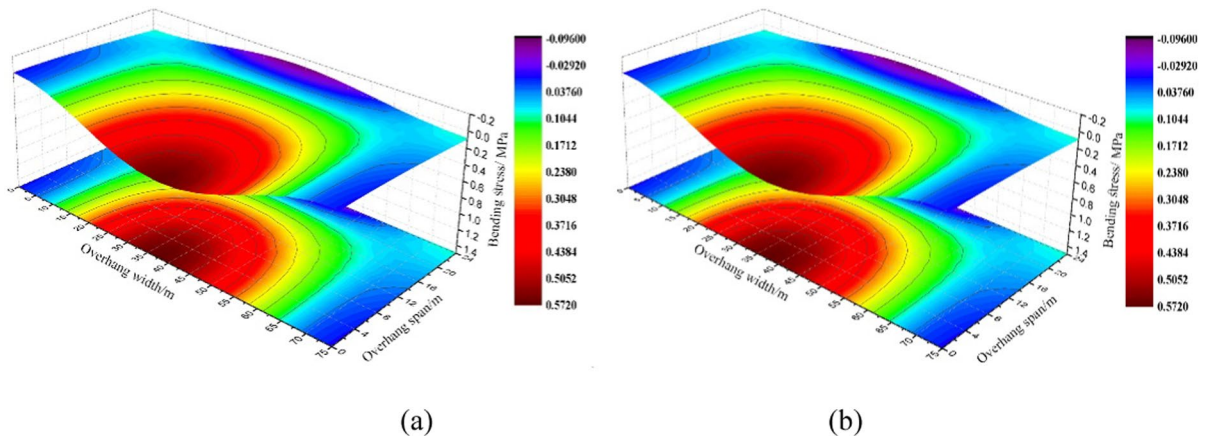


Fig. 20 Bending stress characteristics of the roof along the trend overhang span. **a** $m = 2$ m; **b** $m = 10$ m

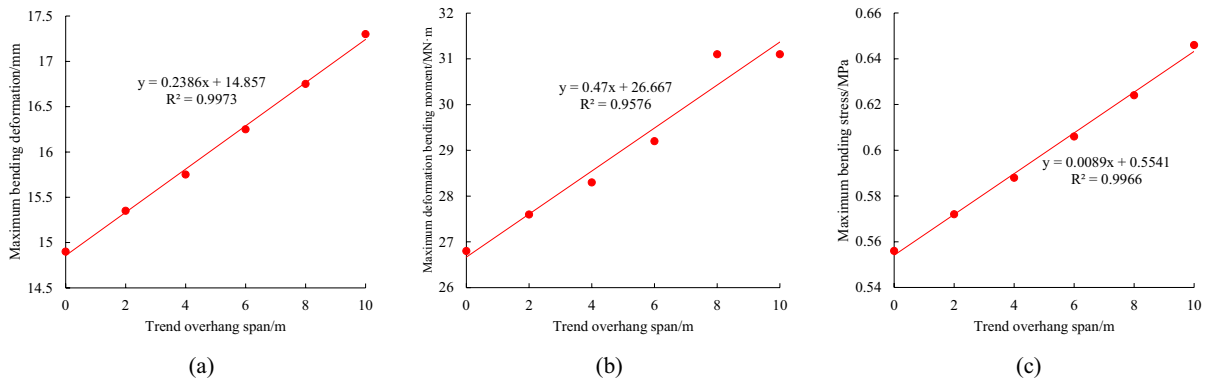


Fig. 21 Curves of maximum bending deformation, deformation bending moment, and bending stress as a function of the trend overhang span. **a** Bending deformation; **b** deformation bending moment; **c** bending stress

Figures 6, 7, 8, 9, 10, 11, 12, 13, 14, 15, 16, 17, 18, 19, 20 and 21 present the results.

4.1 Influence of different overhang widths on the initial fracture of the roof rock stratum

With a constant overhang span of 30 m, Figs. 6, 7 and 8 illustrate the roof’s bending deformation, deformation bending moment, and bending stress characteristics for overhang widths of 75 m and 150 m.

Figures 6, 7 and 8 indicate that the primary bending deformation occurs at the overhang structure’s center during the roof rock layer’s initial fracture stage. The bending moment and bending stress are

predominantly concentrated in the middle section of the structure’s length and at the overhang’s center. These areas are crucial for the onset of fractures and instability.

Given the substantial thickness of the mudstone roof, it offers a significant resistance to bending, causing minor deformation magnitudes under load. However, mechanically, as the roof width increases during the initial fracture phase, the bending deformation and its associated moment and stress exhibit logarithmic growth, as shown in Fig. 9. The regions with the highest bending moment and stress predominantly lie in the structure’s middle length and at the overhang’s center.

4.2 Influence of different overhang spans on the initial fracture of the roof rock stratum

Figures 10, 11 and 12 display the roof rock layer's bending deformation, deformation bending moment, and bending stress characteristics for an overhang width of 75 m under varying overhang spans (10 m and 35 m).

The analysis reveals that during the roof rock layer's initial fracture stage, a 10 m roof span results in a maximum bending deformation of 0.029 mm, a maximum deformation moment of 2.44 MN·m, and a peak bending stress of 0.051 MPa. A smaller overhang span yields a low mechanical response under load. Increasing the span to 15 m results in the bending deformation peaks at 0.145 mm, the deformation moment at 5.4 MN·m, and the stress at 0.113 MPa. As the span expands, the mechanical response intensifies. At a 35 m overhang span, the roof bending deformation tops at 3.96 mm, the deformation moment at 25.4 MN·m, and the bending stress at 0.53 MPa. Overhang span augmentation markedly amplifies the roof bending's mechanical reaction, displaying exponential growth, as indicated in Fig. 13. The overhang span stemming from mining activities directly instigates roof movement and fractures.

4.3 Effect of residual overhanging structures at corners (horizontal overhang span) on periodic fracture of roof rock stratum

Figures 14, 15 and 16 show the roof deformation curve characteristics under various conditions when the fixed overhang structure size (width along the mining face direction, x) is 10 m and the overhang span in the horizontal direction of the working face (y) varies.

When the overhang span along the transverse direction of the working face (y) is 0 m, indicating no residual overhang structure in the transverse direction, the maximum bending deformation of the roof reaches 14.9 mm. The bending deformation mainly occurs in the middle part of the free edge of the overhang structure where the maximum bending moment reaches 26.8 MN·m, and the bending moment is mainly concentrated in the middle part of the fixed support along the long edge of the overhang structure. The maximum bending stress is mainly concentrated

in the middle part of the fixed support along the long edge of the overhang structure with a peak of 0.556 MPa. This middle part of the overhang structure's fixed support along the long edge, namely the middle part of the working face roof, is where fracture instability occurs.

During the periodic fracture phase of the roof rock layer, the corner's residual overhang structure mechanically affects the load-bearing state of the rectangular roof structure, with three sides fixed and one side free. As the overhang span increases, the bending deformation, bending moment, and bending stress all intensify, displaying a robust positive correlation, as illustrated in Fig. 17. The middle part of the fixed support along the long edge of the overhang structure, namely the middle part of the working face roof, is the critical location where fracture instability occurs.

4.4 Effect of residual overhanging structures at corners (trend overhang span) on periodic fracture of roof rock stratum

Figures 18, 19 and 20 present the characteristics of roof deformation curves under different circumstances when the overhang span along the mining direction of the working face (x) changes and the fixed overhang structure size (width along the mining direction, y) is 10 m.

If the width along the mining direction (x) is 0 m, indicating no residual overhang structure in this direction, the maximum bending deformation of the roof is 14.9 mm. The deformation primarily occurs at the overhang structure's free edge center. The maximum bending moment is 26.8 MN·m, concentrated in the center of the overhang structure's long edge along the fixed support. The peak bending stress is 0.556 MPa, primarily located in this area. The overhang structure's long edge center, corresponding to the working face's center, is a crucial fracture instability point.

The study shows that during the periodic fracture stage of the roof rock layer, the mechanical response of the overhang structure amplifies notably with the growth of the overhang span in the mining direction (x). There is a strong positive correlation in bending deformation, bending moment, and bending stress with the overhang span compared to the mechanical response when considering the span's mining direction (y).

In summary, the presence and dimensions of the residual overhang structure significantly influence the roof rock layer’s mechanical behavior and stability during its periodic fracture phase. The overhang span in the mining direction (x) has a more pronounced effect on the mechanical response than the span in the mining direction (y), as illustrated in Fig. 21.

From the case study results, the corner residual overhang structures increase the mechanical stress in the periodic roof structure’s long edge center, leading to fractures and instability. In mining operations, it is vital to consider the roof structure’s periodic overhang, accurately predict the roof’s periodic step distance, and monitor the rear supporting pillars’ stability to ensure the working face’s safe and efficient mining. Adopting such a proactive strategy is imperative to uphold the stability and safety of the working face and supporting pillars during mining operations.

5 Analysis of roof unstable overburden impact and breakthrough step distance estimation

An analysis of the impact of unstable roof overburden in the No. 16705 conventional working face is presented by combining the excavation engineering conditions of the No. 16705 conventional working face with the analysis results of the roof layer’s mining load estimation using the key layer theory. The primary coal seam is approximately 1.0 m thick, and its roof consists, sequentially from the bottom, of a 5.5 m thick gray limestone layer, a 0.7 m thick mudstone layer, a 0.55 m thick gray limestone layer, a 17 m thick mudstone layer, and a 9.7 m thick fine sandstone layer. The 5.5 m gray limestone layer lies within the caving zone, the 17 m mudstone layer resides in the fractured zone, and the 9.7 m fine sandstone layer is situated within the bending zone. During the excavation process of the No. 16705 conventional working face, the first roof layer, the 5.5 m gray limestone layer, undergoes direct roof pressure. Meanwhile, the overlying fifth layer, the 9.7 m thick fine sandstone layer, supports numerous overlying rock layers due to its relative hardness and thickness. However, this layer’s unstable deformation outside the fractured zone minimally influences the mining-induced roof pressure below the working face.

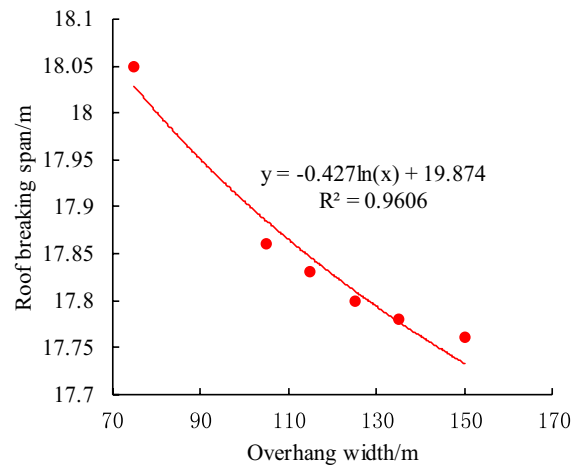


Fig. 22 Variation curve of roof’s initial breakthrough step distance with exposure width

Therefore, the analysis should prioritize the unstable step distance of the 5.5 m gray limestone layer.

Using the key layer theory, the roof layer’s estimated mining load is outlined as follows: the 5.5 m gray limestone layer supports a load of 0.172 MPa, a 0.7 m overlying mudstone layer, and a 0.55 m thick gray limestone layer. The gray limestone layer possesses an elastic modulus of 1.6 GPa, a Poisson’s ratio of 0.2, and a tensile strength of 0.72 MPa. Equations 9 and 30, which determine roof bending stress, are employed to calculate the initial and periodic breakthrough step distances of the roof.

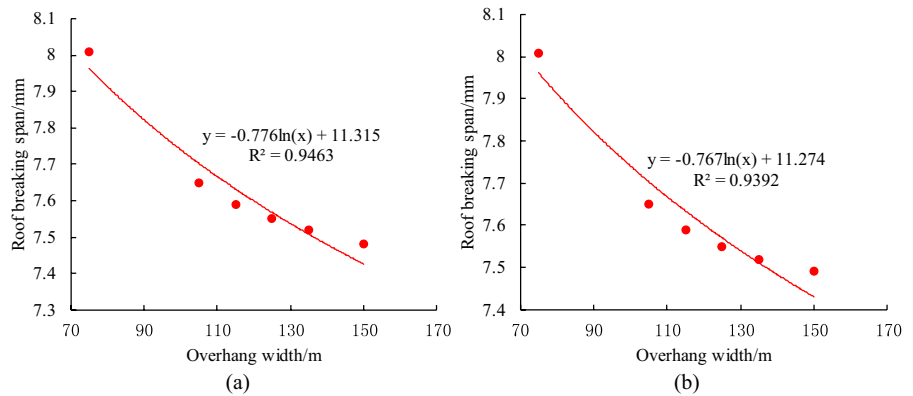
(1) Initial breakthrough step distance of roof movement

$$\begin{aligned}
 M_{x\text{Max}} &= M_x \Big|_{x=0, y=\frac{b}{2}} \\
 &= -\frac{2 \times 0.172}{\pi^2 [3b^4 + 3a^4 + 2a^2b^2]} a^2 b^4 \\
 &\geq -\frac{0.5 \times 5.5^2}{6}
 \end{aligned}$$

The variation in the initial breakthrough step distance of the 5.5 m limestone layer, representing the roof’s first layer, in relation to hanging width, is illustrated in Fig. 22, displaying a logarithmic decline.

(2) Roof movement periodic breakthrough step distance

Fig. 23 Curve of the periodic breakthrough step distance of the roof layer with respect to the exposure width. a $m = 2.0$ m, $l = 1.0$ m; $b = 1.0$ m, $l = 2.0$ m



$$M_{xMax} = M_x \Big|_{x=0, y=\frac{b}{2}}$$

$$= - \frac{0.172 \times \left[32 \times (\pi - 2)a^2b^4 - 64 \times \pi \times \left(1 - \cos \frac{2\pi l}{b} \right) \left(\frac{\pi - 2}{\pi} \right) mlab^3 \right]}{\pi^2 \left[3\pi b^4 + 32a^2b^2(\pi - 4) + 256(3\pi - 8)a^4 \right]} \geq - \frac{0.72 \times 5.5^2}{6} - \frac{8\pi^3 \times 1.6 \times 13.9}{2.31} \left(1 - \cos \frac{2\pi l}{b} \right) \frac{ma^3b^3}{l^3}$$

Figure 23 exhibits the periodic breakthrough step distances of the 5.5 m limestone layer, also representative of the roof’s first layer, in connection with the hanging width, showing a logarithmic decrease.

The theoretical calculations suggest that the roof movement’s initial breakthrough step distance for the topmost 5.5 m gray limestone layer varies between 17.76 and 18.05 m. The roof, having a 75 m short exposure width, is 0.3 m longer than the roof, with a 150 m long exposure width. Similarly, the roof movement’s periodic breakthrough step distance for this layer ranges between 7.48 and 8.01 m. A roof with a 50 m short exposure width is 0.5 m longer than the one with a 150 m long exposure width. Throughout the periodic overburden phase of the mining process, the difference between the 75 m short exposure width roof and the 150 m long exposure width roof becomes evident. The roof fracture instability span increases considerably. In practical mining endeavors, careful consideration must be given to the exposure of the periodic roof structure. Accurate prediction of the roof’s periodic step distance and monitoring the stability of load-bearing pillars behind the working face is essential for ensuring the safe and efficient mining of the working face.

6 Conclusion

This paper combines the engineering geological conditions of the No. 16705 conventional working face, estimates the mining load of the roof rock layer based on the key layer theory, analyzes the mechanical model of the roof rock layer movement of the working face, reveals the influence of different suspended slab structure sizes on the roof movement and its fracture mechanics, analyzes the impact of the unstable weighting of the working face roof, and estimates the roof fracture step distance of the No. 16705 conventional working face, the following conclusions can be drawn:

1. Based on the key stratum theory, analysis of the mining load on the roof layers demonstrates that the 5.5 m thick gray limestone, from bottom to roof, serves as the immediate roof. This immediate roof sustains the load from the succeeding layers: a 0.7 m thick claystone, a 0.55 m thick gray limestone, and a 17 m thick mudstone. Notably, the fifth layer, a 9.7 m thick fine sandstone known for its significant hardness and thickness, plays a vital role in supporting the layers above and is designated as the key stratum for the No. 16705 conventional working face.

2. A comprehensive analysis of both initial and periodic roof breakages was performed by applying the thin plate theory from elasticity mechanics. This analysis shows that, during the periodic roof breakage phase, the long side of the panel structure in the goaf area exists in a simply supported mechanical state. Consequently, the panel structure's mechanical response becomes more pronounced than during the initial roof breakage phase, leading to a heightened risk of fracture instability. In terms of the roof movement's impact on deformation, bending deformation predominantly manifests in the central section of the panel structure's exposure adjacent to the goaf. Thus, ensuring the stability of the load-bearing pillars behind the working face becomes paramount to prevent potential instability.
3. As the width of the roof extends, the maximum bending deformation, deformation moment, and bending stress all exhibit a logarithmic increase. A similar trend is observed with an extended roof exposure span, with exponentially increasing maximum bending deformation, deformation moment, and bending stress. Meanwhile, as the dimensions of the remaining angular protrusions (horizontal and trend overhang spans) expand, the maximum bending deformation, deformation bending moment, and bending stress grow linearly.
4. In the context of the mining conditions at the No. 16705 conventional working face, an analysis concerning the implications of roof instability was carried out. The findings suggest that initial and periodic breakthrough step distances diminish logarithmically as the exposure width expands.

Acknowledgements This work was funded by the National Natural Science Foundation of China under Grant Nos. 51904112 and 51904113. The authors were grateful for the great support awarded.

Author contribution All authors contributed to the study conception and design. Material preparation, data collection and analysis were performed by JZ and QR, the first draft of the manuscript was written by JZ, QR, YY, JC, WS, YY, CW and WL. All authors commented on previous versions of the manuscript. All authors read and approved the final manuscript.

Funding This work was funded by the National Natural Science Foundation of China under Grant Nos. 51904112 and 51904113.

Availability of data and materials The data are contained within this manuscript.

Declarations

Ethics approval and consent to participate Not applicable.

Competing interests The authors declare no competing interests.

Open Access This article is licensed under a Creative Commons Attribution 4.0 International License, which permits use, sharing, adaptation, distribution and reproduction in any medium or format, as long as you give appropriate credit to the original author(s) and the source, provide a link to the Creative Commons licence, and indicate if changes were made. The images or other third party material in this article are included in the article's Creative Commons licence, unless indicated otherwise in a credit line to the material. If material is not included in the article's Creative Commons licence and your intended use is not permitted by statutory regulation or exceeds the permitted use, you will need to obtain permission directly from the copyright holder. To view a copy of this licence, visit <http://creativecommons.org/licenses/by/4.0/>.

References

- Bu QW, Tu M, Zhang XY, Yuan BQ, Zhao QC, Dang JX (2022) Study on fracture instability and energy accumulation-release evolution of thick-hard roof in stope. *J Min Saf Eng* 39(5):867–878
- Duan ZJ, Zheng WX (2022) Study on overlying strata movement and weighting law in shallow coal seam stope. *Coal Technol* 41(11):1–4
- He XQ, Nie BS, He J, Zhai SR (2007) Study on electromagnetic emission characteristics in roof failure. *Chin J Rock Mech Eng* 26(S1):2935–2940
- Hou ZJ (2000) Analysis of combinatorial key strata stability in shallow coal seam with thick loose bed. *J China Coal Soc* 2:127–131
- Hou ZJ (2001) Study on application of combinatorial key stratum theory and parameters deter mining. *J China Coal Soc* 6:611–615
- Hou EK, Chen Y, Che XY, Xie XS, Gao B (2021) Study on overburden failure characteristics and fracture evolution law of shallow buried coal seam through trench mining. *Coal Sci Technol* 49(10):185–192

- Huang QX, Tang PF (2017) Roof structure analysis on large mining height longwall face in shallow coal seam. *J Min Saf Eng* 34(2):282–286
- Huang QX, Zhao MY, Huang KJ (2019) Study of roof double key strata structure and support resistance of shallow coal seams group mining. *J China Univ Min Technol* 48(1):71–77+86
- Jiang HJ, Cao SG, Zhang Y, Wang C (2016) Study on the first failure and caving mechanism of key strata of shallow coal seam. *J Min Saf Eng* 33(05):860–866
- Li JH (2017) Research on the law of overburden failure and surface movement in shallow seam. Xi'an University of Science and Technology, Xi'an
- Ma Q, Liu XL, Tan YL, Elsworth D, Shang JL, Song DQ, Liu XS, Yan FY (2023) Numerical study of mechanical properties and microcrack evolution of double-layer composite rock specimens with fissures under uniaxial compression. *Eng Fract Mech* 289(2):109403
- Ning JG, Wang J, Tan YL, Xu Q (2020) Mechanical mechanism of overlying strata breaking and development of fractured zone during close-distance coal seam group mining. *Int J Min Sci Technol* 30(2):207–215
- Pang YH, Wang HB, Lou JF, Chai HL (2022) Longwall face roof disaster prediction algorithm based on data model driving. *Int J Coal Sci Technol* 9(1):11
- Przyłucka M, Kowalski Z, Perski Z (2022) Twenty years of coal mining-induced subsidence in the Upper Silesia in Poland identified using InSAR. *Int J Coal Sci Technol* 9(1):86
- Qian GM (2017) Strengthening theoretical research on coal mining and realizing scientific mining. *J Min Saf Eng* 34(4):615
- Qian MG, Xu JL (2019) Behaviors of strata movement in coal mining. *J China Coal Soc* 44(4):973–984
- Ren YF (2020) Spatiotemporal evolution process of full thickness cutting of roof bedrock layer in shallow buried working face. *J China Coal Soc* 45(S2):561–570
- Song ZQ, Jiang YJ, Liu JK (2017) Theory and model of “practical method of mine pressure control.” *Coal Sci Technol Mag* 2:1–10
- Song ZQ, Hao J, Shi YK, Tang JQ, Liu JK (2019) An overview of connotation and development of practical ground pressure control theory. *J Shandong Univ Sci Technol (nat Sci)* 38(1):1–15
- Sun YJ, Zou JP, Murat K, Wang JT (2019) Investigation of movement and damage of integral overburden during shallow coal seam mining. *Int J Rock Mech Min Sci* 117:63–75
- Tan YL, Ma Q, Liu XL, Liu XS, Elsworth D, Qian RP, Shang JL (2023) Study on the disaster caused by the linkage failure of the residual coal pillar and rock stratum during multiple coal seam mining: mechanism of progressive and dynamic failure. *Int J Coal Sci Technol* 10:45
- Wang XF, Lu MY (2022) Study on mechanical mechanism of roof fracture evolution in deep stope with variable face length. *Coal Geol Explor* 50(10):1–15
- Wang BF, Liang B, Sun KM, Wu ZC, Sun WJ, Jiang LG, Wang JG (2017) Research on overlying strata response and control during typical shallow coal seam longwall mining. *Rock Soil Mech* 38(9):2693–2700
- Wei JB, Wang SM, Song SJ, Sun Q, Yang T (2022) Experiment and numerical simulation of overburden and surface damage law in shallow coal seam mining under the gully. *Bull Eng Geol Environ* 81:207
- Xu JL, Zhu WB, Wang XC, Yi MS (2009) Classification of key strata structure of overlying strata in shallow coal seam. *J China Coal Soc* 34(7):865–870
- Yuan FZ, Ma K, Tang CA, Wang SJ, Guo HY (2022) Movement of overburden with different mining thickness and reponse characteristics of surrounding rock under multi-key layer structure. *Coal Sci Technol* 50(6):211–218
- Zhang Z, Li JG (2021) Study on ground pressure law of super long working face in shallow coal seam. *Coal Sci Technol* 49(S2):30–33
- Zhang J, He MC, Hideki S, Wang YJ, Hou SL, Liu B, Yang G, Zhou P, Li HC, Wu X (2023) Similar model study on the principle of balanced mining and overlying strata movement law in shallow and thin coal seam based on N00 mining method. *Eng Fail Anal* 152:107457
- Zhao J, Liu CY, Li JW (2017) Overburden failure and strata pressure behavior characteristics under condition of shallow coal seam in gully terrain. *Coal Sci Technol* 45(1):34–40
- Zhao YH, Zhou CH, Zhang X, Yuan C (2020) The pressure arching effect and distribution characteristics of fractured strata of single key layer under shallow buried condition. *J China Coal Soc* 45(S1):1–11
- Zhou JL, Huang QX (2019) Stability analysis of key stratum structures of large mining height longwall face in shallow coal seam. *Chin J Rock Mech Eng* 38(7):1396–1407
- Zuo JP, Sun YJ, Wen JH, Li ZD (2018) Theoretical and mechanical models of rock strata movement and their prospects. *Coal Sci Technol* 46(1):1–11+87

Publisher's Note Springer Nature remains neutral with regard to jurisdictional claims in published maps and institutional affiliations.